

RESEARCH

Open Access



Increased temperature enhances microbial-mediated lignin decomposition in river sediment

Jialing Li^{1,2}, Weimin Sun³, Yingjie Cao¹, Jiayue Wu¹, Li Duan¹, Miaomiao Zhang⁴, Xiaoqing Luo¹, Qiqi Deng¹, Ziqi Peng¹, Xiaozhen Mou⁵, Wenjun Li^{1*} and Pandeng Wang^{1,6*}

Abstract

Background Lignin, as the most abundant recalcitrant organic carbon in terrestrial ecosystems, plays a crucial role in the Earth's carbon cycle. After lignin entering aquatic environments, portion of it tends to accumulate in sediments, forming a stable carbon relatively reservoir. However, the increasing temperature caused by human activities may impact microbial-mediated lignin decomposition, thereby affecting sedimentary carbon reservoirs. Therefore, revealing how temperature affects microbial-mediated lignin decomposition in river sediment, a topic that remains elusive, is essential for comprehending the feedbacks between river carbon reservoirs and climate. To address this, we conducted stable isotope probing of river surface sediment using ¹³C-lignin and ¹³C-vanillin, and utilized a series of techniques, including CO₂ production analysis, 16S rRNA gene amplicon sequencing, metagenomics, and metatranscriptomics, to identify the lignin-decomposing microbes and the effects of temperature on microbial-mediated lignin decomposition.

Results We found that elevated temperatures not only increased the total sediment respiration (total CO₂) and the CO₂ emissions from lignin/vanillin decomposition, but also enhanced priming effects. The ¹³C-labeled taxa, including *Burkholderiales*, *Sphingomonadales*, and *Pseudomonadales*, were identified as the main potential lignin/vanillin decomposers, and their abundances and activity significantly increased as temperature increased. Furthermore, we observed that increasing temperature significantly increased the activity of lignin decomposing pathways, including *β-aryl ether fragments* and *4,5-PDOG pathway*. Additionally, as temperature increases, the transcriptional abundances of other carbon cycling related genes, such as *pulA* (starch decomposition) and *xylA* (hemicellulose decomposition), also exhibited increasing trends. Overall, our study elucidated the potential lignin-decomposing microbes and pathways in river sediment and their responses to temperature increasing.

Conclusions Our study demonstrated that the temperature increasing can increase the rate of lignin/vanillin decomposition via affecting the activity of lignin-decomposing microbes. This finding indicates that the ongoing intensification of global warming may enhance the decomposition of recalcitrant organic carbon in river sediment, thereby impacting global carbon cycling.

Keywords Lignin decomposition, Temperature increasing, Carbon cycling, Lignin decomposers and pathways

*Correspondence:

Wenjun Li

liwenjun3@mail.sysu.edu.cn

Pandeng Wang

wangpd@mail2.sysu.edu.cn

Full list of author information is available at the end of the article



© The Author(s) 2025. **Open Access** This article is licensed under a Creative Commons Attribution-NonCommercial-NoDerivatives 4.0 International License, which permits any non-commercial use, sharing, distribution and reproduction in any medium or format, as long as you give appropriate credit to the original author(s) and the source, provide a link to the Creative Commons licence, and indicate if you modified the licensed material. You do not have permission under this licence to share adapted material derived from this article or parts of it. The images or other third party material in this article are included in the article's Creative Commons licence, unless indicated otherwise in a credit line to the material. If material is not included in the article's Creative Commons licence and your intended use is not permitted by statutory regulation or exceeds the permitted use, you will need to obtain permission directly from the copyright holder. To view a copy of this licence, visit <http://creativecommons.org/licenses/by-nc-nd/4.0/>.

Background

Rivers are important reservoirs of organic carbon on the earth [1–4]. Recent years, climate change is increasing the global river water temperature, making the river carbon pool become vulnerable to microbial decomposition [5–7]. Compared with chemically labile carbon, the recalcitrant carbon is reported to be more vulnerable to the temperature changes [8]. Therefore, the chemically recalcitrant carbon in river sediment may serve as a noteworthy source of greenhouse gases with the intensification of global warming.

Lignin, derived from terrestrial plant cells, constitutes the most abundant recalcitrant organic carbon on land [9]. Approximately 60% of the terrestrial lignin were transported into river, where it was decomposed into smaller components during being transported to ocean or buried in sediments [10]. In river ecosystems, the mineralization of lignin was mainly carried out by heterotrophic microorganisms [10, 11]. It was shown that various bacteria, fungi, and archaea (spanning over 90 different genera) can decompose lignin and lignin-derived aromatic compounds [12–15]. As bacteria are the dominant microorganisms in river sediment and can utilize diverse terminal electron receptors during the decomposition of refractory carbon [16, 17], they may play an important role in the decomposition of recalcitrant organic carbon (e.g., lignin) in the river ecosystems. Previous studies have demonstrated that bacteria (e.g., *Burkholderia*) were the dominate lignin decomposers in tundra or forest soils and warming could significantly accelerated lignin decomposition [18, 19]. However, it is still elusive about how microbial-mediated lignin decomposition in river sediment responses to temperature changes, which is essential for comprehending the feedback between river carbon reservoirs and climate. Here, we hypothesized that increasing temperature would enhance the release of CO₂ derived from lignin via altering the abundances and metabolic activity of lignin decomposers and promoting specific lignin decomposition pathways in the river sediment.

Results

Increased temperature enhanced the sediment respiration, lignin/vanillin decomposition, and priming effect

To investigate the effects of temperature on lignin decomposition, we conducted stable isotope probing (SIP) experiments using ¹³C-labeled lignin and ¹³C-labeled vanillin under three temperature conditions (23 °C, 26 °C, and 29 °C) (Fig. 1a; Table S1; Table S2). ¹³C-lignin was utilized to signify the initial stages of HMW lignin decomposition, during which lignin macromolecular polymers are broken down into smaller aromatic compounds. In contrast, ¹³C-vanillin was employed to denote

the later stages of lignin decomposition, specifically the ring cleavage of these aromatic compounds. As temperature increased, the production rate of accumulated total CO₂ significantly increased from the last day among different treatment groups (Fig. 1c, g; one-way ANOVA, $P < 0.05$). Meanwhile, the cumulative ¹³CO₂ derived from ¹³C-labeled lignin/vanillin was also significantly higher during the incubation when temperature increased (Fig. 1b, f; one-way ANOVA, $P < 0.05$). Furthermore, we also found that the ratio of CO₂ coming from ¹³C-labeled lignin exhibited an increasing trend as temperature increased (Fig. 1d, h). These indicate that increasing temperature may have a stronger effect on lignin decomposition than other organic carbons. Additionally, we observed a strong priming effect due to the addition of lignin or vanillin, and this priming effect could be significantly enhanced by increasing temperature (Fig. 1e, i; one-way ANOVA, $P < 0.05$).

Increased temperature affected the abundance and activity of lignin/vanillin decomposers

To identify lignin decomposers and their responses to temperature increasing, SIP experiments were performed. The peak of ¹³C-labeled DNA was detected around the fraction buoyant density of 1.736 g/mL (heavy fraction, Fig. S1 and S2), which presented only in ¹³C-lignin/¹³C-vanillin incubation samples, but not in ¹²C-lignin/¹²C-vanillin incubation samples and no vanillin/lignin samples. The peak concentration of ¹²C-labeled DNA was detected around the density of 1.702 g/mL (light fraction). The total abundance of ¹³C-lignin-labeled microbes significantly (Kruskal Wallis test, $P < 0.05$) increased from $(1.06 \pm 0.06) \times 10^7$ copies/g sediment to $(1.93 \pm 0.20) \times 10^7$ copies/g sediment as temperature increased from 23 to 29 °C (Fig. 2a). Temperature significantly influenced both vanillin and lignin decomposers; however, its impact on vanillin decomposers was notably more pronounced, particularly at 29 °C (Fig. 2b; Kruskal–Wallis test, $P < 0.05$). Additionally, we found that the community compositions of potential lignin/vanillin decomposers significantly changed as the temperature increased based on Bray–Curtis distance (Figs. 2cd, S3, and S4; PERMANOVA, $P < 0.05$).

We identified the potential lignin/vanillin decomposers from the ¹³C-labeled DNA fraction and found that they could be grouped into four clusters (I, II, III, and IV) according to the phylogenetic tree of them (Fig. 3). These clusters included orders *Burkholderiales*, *Pseudomonadales*, *Sphingomonadales*, *Anaerolineales*, *Gemmatimonadales*, *Clostridiales*, *Actinomycetales*, *Myxococcales*, *Deinococcales*, etc. Cluster I was exclusively consisted of *Burkholderiales* (β -*Proteobacteria*), and the relative abundance of five ASVs significantly increased

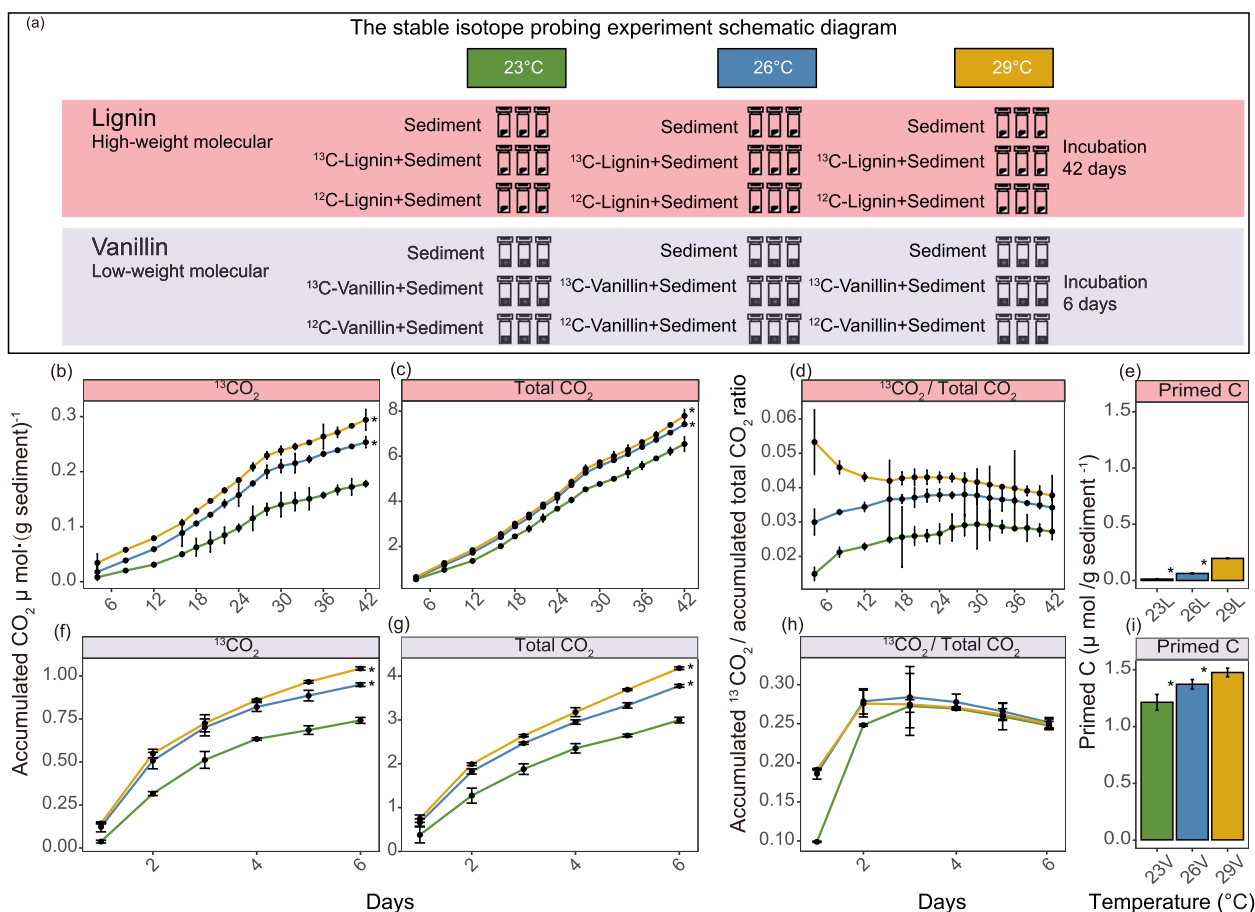


Fig. 1 The effect of temperature on lignin/vanillin decomposition. **a** The stable isotope probing experiment schematic diagram. The accumulated ¹³CO₂, accumulated total CO₂, ratio of accumulated ¹³CO₂/accumulated total CO₂, and the priming effect during lignin incubation (**b, c, d, e**) and vanillin incubation (**f, g, h, i**). 23 °C: green lines/bars; 26 °C: blue lines/bars; 29 °C: orange lines/bars. The differences of CO₂ and primed C amounts among different temperature treatments were determined by one-way ANOVA ($n=3$; $*P<0.05$). Data were shown as mean \pm SD

with the increasing temperature (Fig. 3; ALDEx2, $P<0.05$). In ¹³C-lignin-labeled DNA, the absolute abundance of *Burkholderiales* significantly increased from $(0.82 \pm 0.031) \times 10^6$ copies/g, $(1.06 \pm 0.028) \times 10^6$ copies/g to $(1.23 \pm 0.019) \times 10^6$ copies/g as temperature increased from 23 °C, 26 °C to 29 °C (Fig. 2b; Kruskal–Wallis test, $P<0.05$). Similarly, in ¹³C-vanillin-labeled DNA, the absolute abundances of *Burkholderiales* also significantly increased with increasing temperature (Fig. 2b; Kruskal–Wallis test, $P<0.05$). To further demonstrate their lignin-decomposing capability, we recovered 11 MAGs (Metagenome-Assembled Genomes) belonging to *Burkholderiales* from the metagenomic data. Among them, nine MAGs encoded lignin peroxidases, which directly participate in the depolymerization of lignin (Table S3 and S4). Notably, the abundances of bin37 (*Pandoraea*), bin47 (*Cupriavidus*) and bin48 (*Cupriavidus*) significantly increased with the increasing temperature (Table S4 and S5; ALDEx2, $P<0.05$).

Cluster II was primarily consisted of the order *Pseudomonadales* (*Gammaproteobacteria*). The relative abundance of *Pseudomonas*, including ASV12, ASV130, and ASV133, in the ¹³C-vanillin-labeled DNA significantly decreased with increasing temperature (Fig. 3; ALDEx2, $P<0.05$). The relative abundance of the *Pseudomonadales* order also exhibited a decreasing trend with increasing temperature (Fig. S4), while its absolute abundance increased from $(0.67 \pm 0.013) \times 10^6$ copies/g and $(0.047 \pm 0.014) \times 10^6$ copies/g to $(1.41 \pm 0.015) \times 10^6$ copies/g as temperature increased from 23 °C and 26 °C to 29 °C (Fig. 2b). Additionally, we recovered 19 *Pseudomonadales* MAGs from our metagenomic data (Table S5), and these MAGs encoded genes involved in the intermediate metabolism of lignin decomposition. The abundance of bin23 (*Pseudomonas*) significantly increased with the increasing temperature; however, the abundances of bin19 (*Pseudomonas*) and bin33 (*Pseudomonas*) significantly decreased with increasing

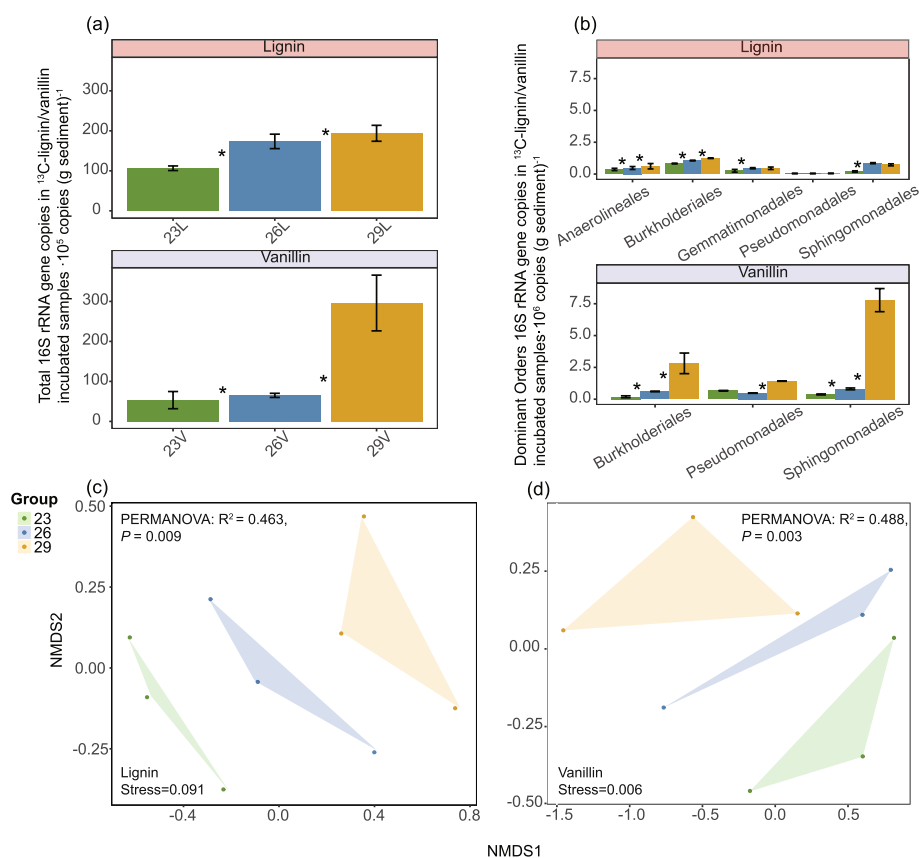


Fig. 2 Responses of potential lignin/vanillin microbial decomposers to increasing temperature. **a** The changes in absolute abundances of ¹³C-labeled microbial communities along temperature gradient. qPCR was used to determine the absolute abundances of microbial communities in heavy fractions (¹³C-labeled) under different incubation treatments. **b** The responses of the abundances of ¹³C-labeled dominant orders to increasing temperature. NMDSS showed the composition changes of potential (¹³C-labeled) lignin (**c**) or vanillin (**d**) decomposers across different temperature treatments. The significances of differences were determined by Kruskal Wallis test and PERMANOVA ($n = 3$; $*P < 0.05$). Data were shown as mean \pm SD

temperature (Table S4; ALDEx2, $P < 0.05$). Furthermore, a strain of *Pseudomonadales* (*Pseudomonas aeruginosa*) was isolated from the Pearl River sediment with lignin as the sole carbon source (Table S6).

Cluster III was primarily consisted of the order *Sphingomonadales* (*Alphaproteobacteria*). The relative abundances of the two ASVs significantly increased with increasing temperature (Fig. 3; ALDEx2, $P < 0.05$). In the ¹³C-lignin-labeled DNA, the absolute abundance of *Sphingomonadales* increased from $(0.19 \pm 0.055) \times 10^6$ copies/g to $(0.85 \pm 0.043) \times 10^6$ copies/g and $(0.72 \pm 0.079) \times 10^6$ copies/g as temperature increased from 23 °C to 26 °C and 29 °C (Fig. 2b). Similarly, in the ¹³C-vanillin-labeled DNA, the absolute abundance of *Sphingomonadales* also significantly increased with increasing temperature (Fig. 2b). We recovered 12 MAGs belonging to the order *Sphingomonadales* from our metagenomic data (Table S4), and these MAGs encoded genes involved in the intermediate metabolism of lignin

decomposition. In consistent with the ASV results, the abundances of bin7 (*Sphingobium*) and bin14 (*Novosphingobium*) significantly increased with increasing temperature (Table S4; ALDEx2, $P < 0.05$). Additionally, we also isolated a strain belonging to the *Sphingomonadales* order (*Aestuariusphingobium littorale*) using a culture medium with lignin as the sole carbon source and found that its genome encoded ligninolytic genes, including the high-molecular-weight lignin-metabolizing enzymes β -etherase (*ligEFG*) and ring-cleaving enzymes (*ligM*, *ligB*, etc.) (Table S6), which provided further evidence for the lignin decomposing ability of *Sphingomonadales*.

Increased temperature changed the lignin decomposition pathways

Based on the literature pertaining to lignin decompositions, we constructed the potential pathways of lignin/vanillin decomposition (Figs. 4 and 5; Fig. S5). Our results revealed that temperature could strongly affect

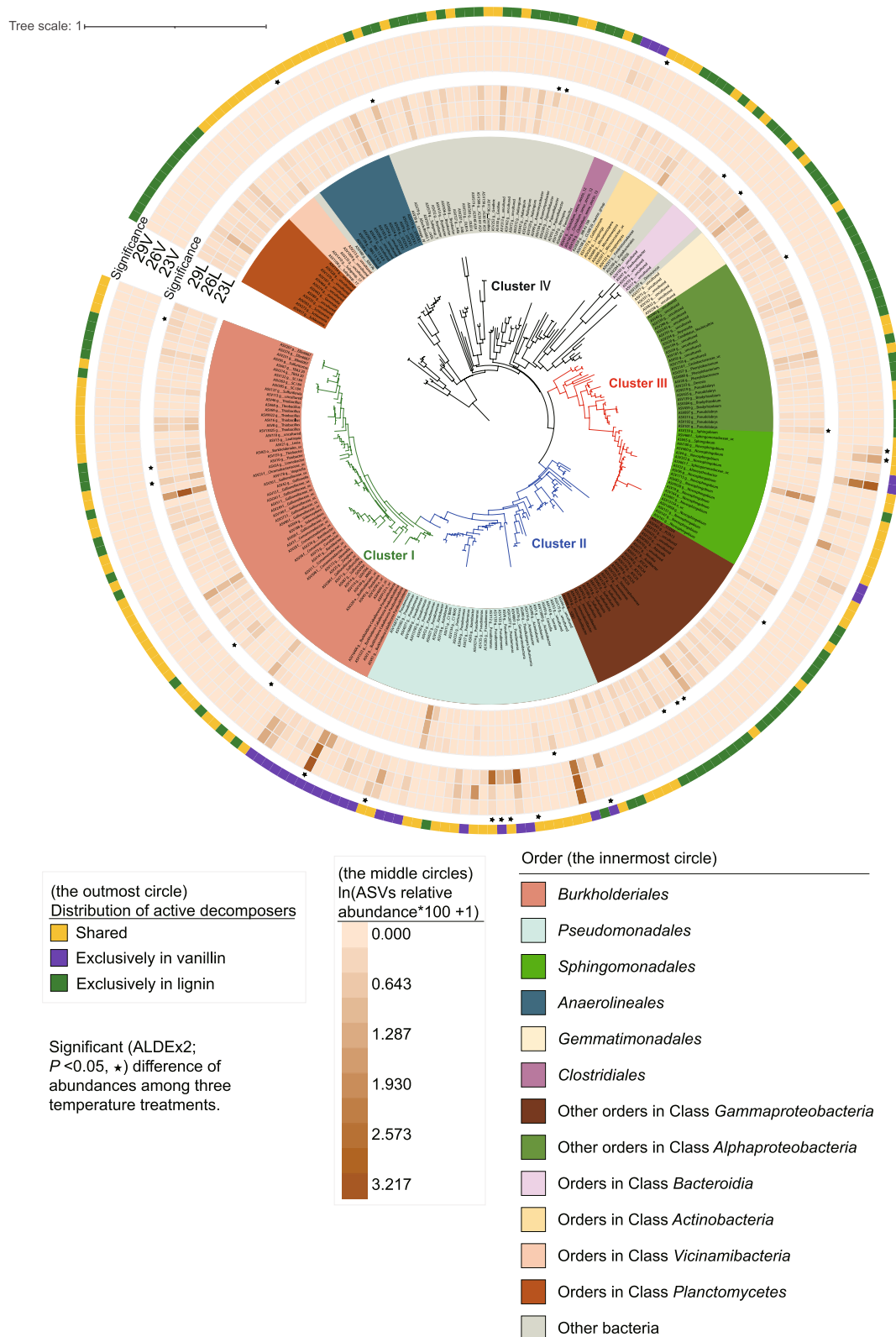


Fig. 3 The maximum likelihood phylogenetic tree of the ^{13}C -labeled potential lignin/vanillin decomposers. Relative abundances of the lignin/vanillin decomposers (amplicon sequence variants, ASVs) were identified based on ^{13}C -DNA (see the "Methods" section for details)

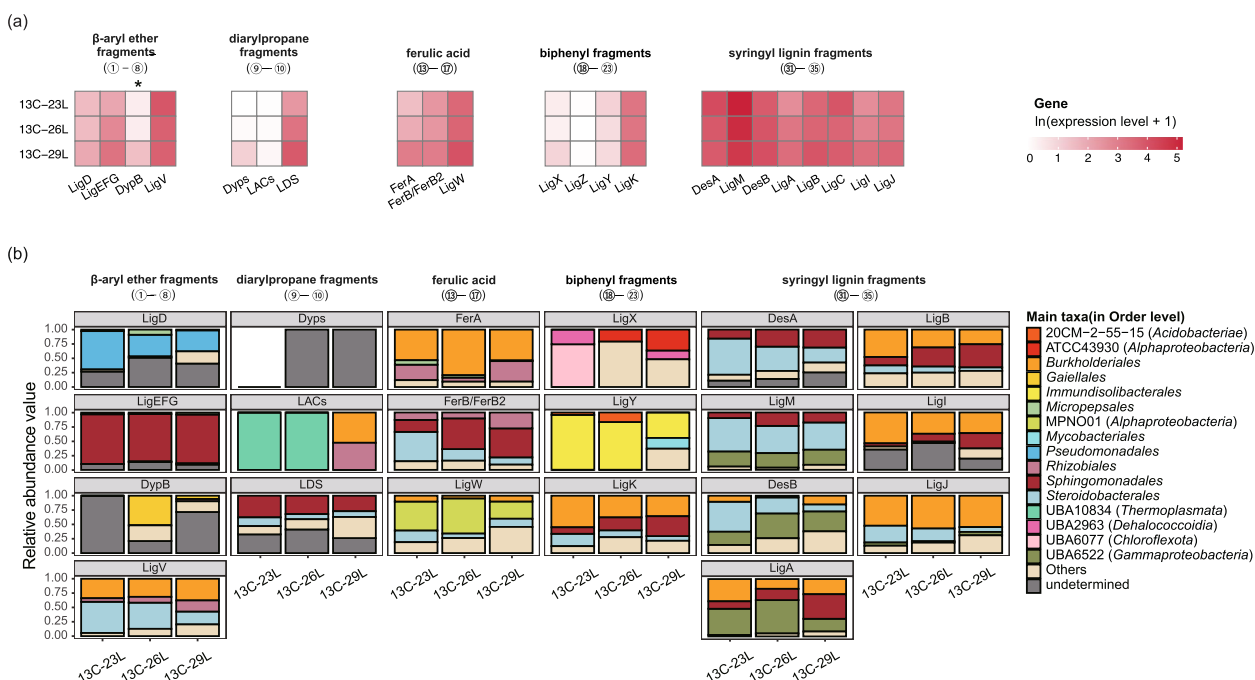


Fig. 4 The effects of temperature on lignin decomposition pathways and potential microbial decomposers. **a** Lignin decomposition pathways under different temperatures (see Fig. S5a). The changes of normalized gene abundances in total RNA across three treatments were showed by heatmap. ALDEx2 test was used to determine the significant difference of abundances among three temperature treatments (* $P < 0.05$). **b** Taxonomic compositions of lignin-decomposing genes. The reference genes of these steps were listed in Table S3

the expressions of functional genes involved in these pathways and the compositions of major decomposers that encoding these functional genes (Figs. 4 and 5). As for the decomposition of high molecular weight (HMW) lignin, we found that the activity of some decomposing pathways, including β -aryl ether fragments (Steps ①-⑧) (ALDEx2, $P < 0.05$), diarylpropane fragments (Steps ⑨-⑩), ferulic acid fragments (Steps ⑬-⑰), increased as the temperature increased, while the activity of decomposing pathways of biphenyl fragments (Steps ⑱-⑳) and syringyl lignin fragments (Steps ㉓-㉕) decreased with the increasing temperature. As for the decomposition of low molecular weight (LMW) vanillin, we found that the activity of common pathway (Step ㉔) and 4,5-PDOG pathway (Steps ㉖-㉚) significantly increased as temperature increasing (ALDEx2, $P < 0.05$), while the transcriptional abundances of genes (except for *pcaB* in Step ㉛) involved in 3,4-PDOG pathway (Steps ㉞-㉟) significantly decreased with increasing temperature (ALDEx2, $P < 0.05$). Additionally, the transcriptional abundances of several genes (Steps ㊱*praA*, Steps ㊲*praH*, and Steps ㊳*praE*) involved in 2,3-PDOG pathway (Steps ㊴-㊶) were zero, indicating that this pathway may be not active in our study environment.

According to the taxonomy classification of functional genes involved in the decomposition of HMW lignin, we found that the main decomposers of each step were obviously different and diverse, and their relative contributions (transcriptional abundances) changed as temperature increased (Fig. 4b). As for the LMW vanillin decomposition pathway, the decomposers mainly distributed in *Burkholderiales*, *Sphingomonadales*, and *Pseudomonadales*, although their relative contributions changed across different steps and temperature conditions (Fig. 5b).

Increased temperature caused the broad changes of carbon-decomposing

Except for lignin decomposition, we also observed a significant increase in the expression levels of other C-decomposing genes (Fig. 6; Fig.S6). Notably, the transcriptional abundances of genes associated with decompositions of starch (*pulA*-Pullulanase), hemicellulose (*xyla*- Xylose isomerase), terpene (*limeh*), and chitin (acetylglucosaminidase) exhibited a substantial increase (1.06~6.67-fold) in ¹³C-vanillin-labeled DNA when temperature increased 3 or 6 °C (Fig. 6). In contrast, the transcriptional abundances of several genes, including

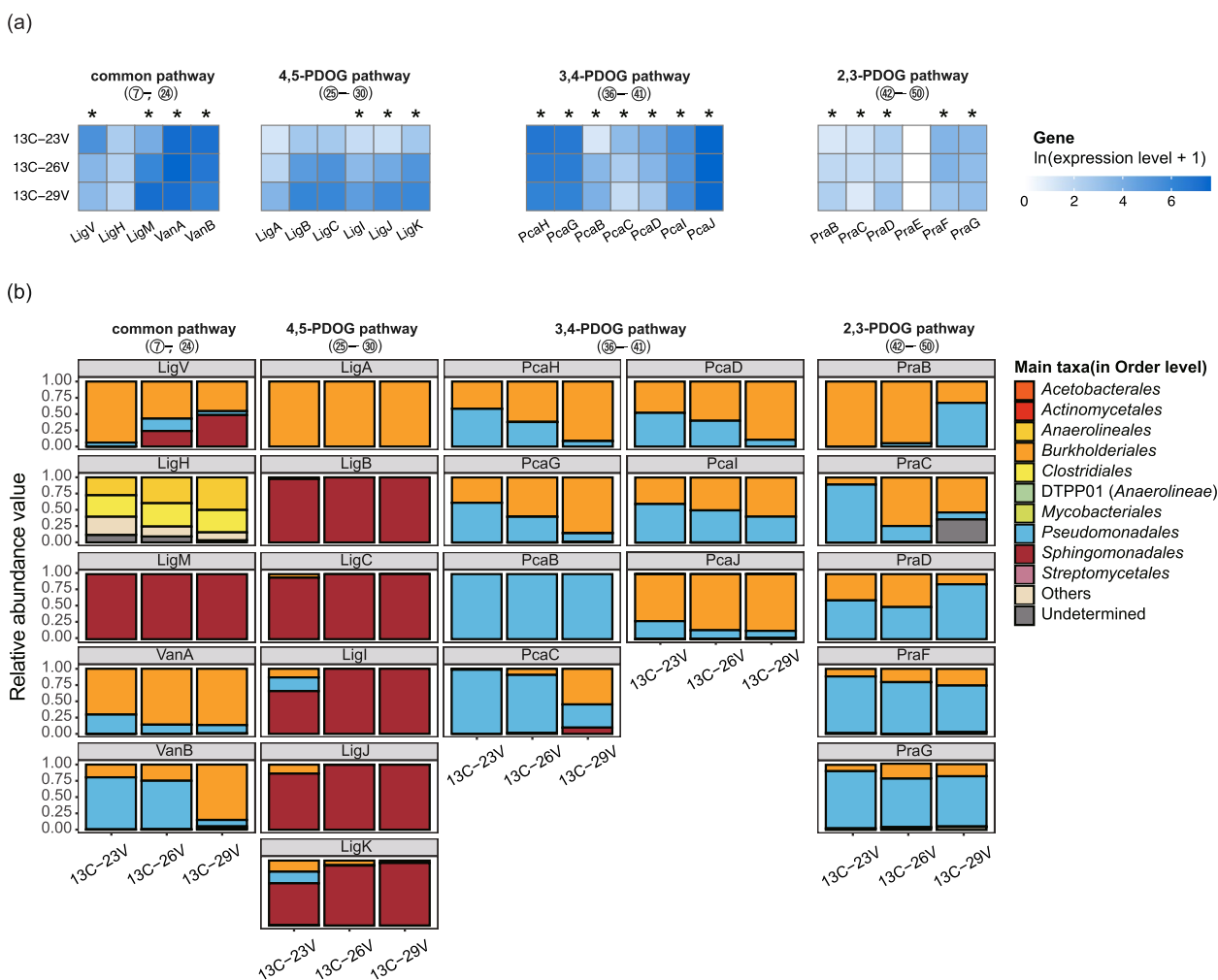


Fig. 5 The effects of temperature on vanillin decomposition pathways and potential microbial decomposers. **a** Vanillin decomposition pathways under different temperatures (see Fig. S5a). The changes of normalized gene abundances in total RNA across three treatments were showed by heatmap. ALDEx2 test was used to determine the significant difference of abundances among three temperature treatments (* $P < 0.05$). **b** Taxonomic compositions of vanillin-decomposing genes. The reference genes of these steps were listed in Table S3

endoglucanase, exhibited a significant decrease as the temperature increased (Fig. 6). These results suggest that increasing temperature could affect the decomposition of a wide range of organic carbon.

Discussion

In this study, we used two substrates (^{13}C -lignin and ^{13}C -vanillin) for SIP incubation experiments with the following reasons. Lignin decomposition is commonly divided into two stages: (1) the decomposition of the macromolecular polymer of lignin into smaller aromatic compounds and (2) the subsequent ring cleavage process of these aromatic compounds [13, 14, 20]. In natural environments, lignin exists in different forms including lignin macromolecules and LMW lignin (e.g., vanillin)

with different degrees of oxidation [10, 21, 22]. The presences of ether and C–C linkages in lignin make it highly resistant to hydrolytic attack, rendering it difficult to break down [14]. Consequently, lignin decomposition in natural conditions is a time-consuming process. In addition, a significant portion of lignin was transported into rivers in the form of LMW lignin with different degrees of oxidation [21, 23]. Therefore, only using ^{13}C -lignin macromolecules for incubation experiments may lead to a skewed understanding of effects of increasing temperature on microbial-mediated lignin decomposition. The key intermediate in the decomposition of LMW lignin is vanillin or vanillic acid, which is commonly used as model aromatic substance in previous studies to investigate lignin decomposition processes [13, 24–26]. Thus, in

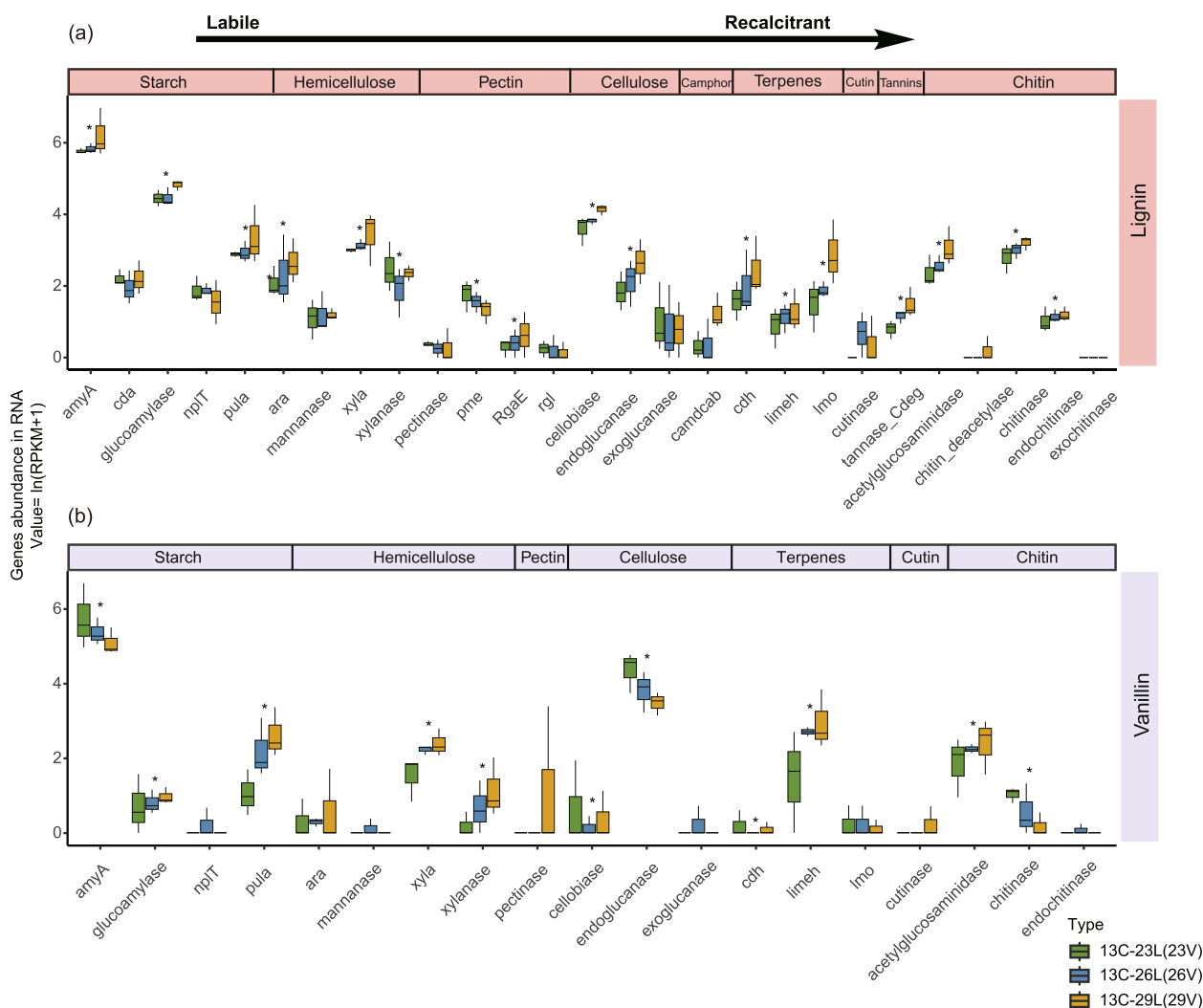


Fig. 6 The changes of normalized transcriptional abundances of key C-decomposing genes in ¹³C-labeled microbial communities (**a** lignin; **b** vanillin). From left to right, the potential substrates of the decomposing genes exhibit a gradual transition from easily degradable to more challenging to be decomposed. Differences in gene abundances were determined using Kruskal Wallis test (**P* < 0.05)

this study, ¹³C-lignin was used to indicate the early stage of HMW lignin decomposition, while ¹³C-vanillin was used to indicate the decomposition of LMW lignin in the later stage.

According to the SIP experiments, we found that the production rate of total CO₂ significantly increased as the temperature increased, indicating that the respiration of organic carbon by the whole microbial community was augmented by the increasing temperature. The decomposition of lignin/vanillin was also significantly enhanced by increasing temperature with the evidence that the cumulative ¹³CO₂ derived from ¹³C-labeled lignin/vanillin was greater in higher temperature conditions. Moreover, the lignin decomposition may be more vulnerable to temperature increasing than other organic carbons, given

that the ratio of CO₂ coming from ¹³C-labeled significantly increased as the temperature increased. Consistently, previous study also found that the decomposition of chemically recalcitrant carbon could be accelerated by 21% when the temperature increased by 2 °C, while only a 10% rise was observed for chemically labile carbon in global soils [8]. Additionally, the priming effects of lignin/vanillin addition were also significantly enhanced by increasing temperature, suggesting that as global warming intensified, the input lignin/vanillin from lands would more strongly stimulate the decomposition of organic carbon in river sediment (Fig. 7), which may release more greenhouse gases and boost climate change.

We further revealed the potential mechanisms underlying this phenomenon. In line with previous studies [18,

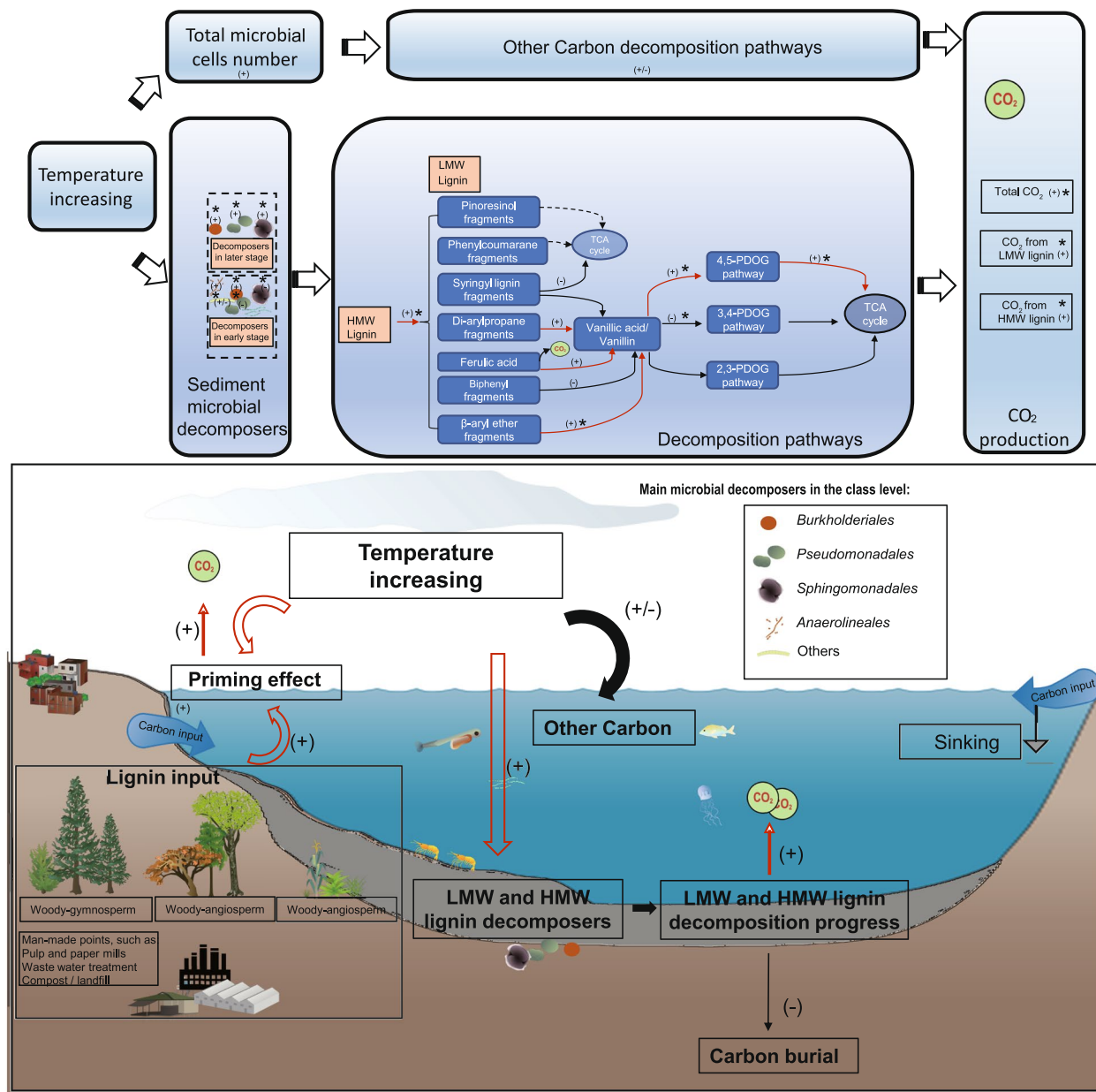


Fig. 7 Conceptual diagram showing the effects of temperature increasing on lignin decomposition and carbon cycling in river sediments. Human activities result in higher discharges of dissolved or particulate matter and organic carbon (including lignin) into the rivers, which could increase the carbon accumulation in the sediments. As temperature increased, the total microbial cells and the abundance of lignin decomposers increased, which enhanced the microbes-mediated decomposition of lignin, CO₂ production, and priming effect within the sediments. The dynamics in both high molecular weight (HMW) and low molecular weight (LMW) lignin decomposition indicate the high sensitivity of carbon cycling to increasing temperature. The plus (+) symbol indicates an increasing effect, while the minus (-) symbol indicates a decreasing effect. ALDex2, *P < 0.05

27–33], we found that the microbial community compositions were significantly altered by temperature change, and the abundances of total lignin/vanillin decomposers significantly increased as the temperature increased. The increasing abundance of decomposers could be responsible for the enhanced decomposition of lignin/vanillin

(higher cumulative CO₂ at greater temperature). In the ¹³C-labeled DNA, we determined that *Burkholderiales* and *Sphingomonadales* were the potential key lignin/vanillin decomposers. Additionally, we recovered 11 *Burkholderiales* MAGs and 12 *Sphingomonadales* MAGs from metagenomic data. Utilizing genome analyses, we

found that 9 *Burkholderiales* MAGs encoded lignin peroxidases, confirming their roles in the depolymerization of lignin. Meanwhile, all recovered *Sphingomonadales* MAGs encoded genes that are involved in the intermediate metabolism of lignin. Using lignin as the sole carbon source, we also isolated a strain (genus *Aestuariusphingobium*) of the *Sphingomonadales* order and confirmed that this strain contained lignin-decomposing related genes, which further demonstrated that *Sphingomonadales* could decompose lignin. Consistent with our findings, *Novosphingobium* (order *Sphingomonadales*) has also been identified as active lignin decomposers in forest soils across North America [19]. Furthermore, after 42 days (^{13}C -lignin) and 7 days (^{13}C -vanillin) incubations, the absolute abundances of *Burkholderiales*, *Sphingomonadales* increased by 1.26~15 and 2.27~20.9 times respectively when temperature increased from 23 °C to 26 °C and 29 °C (Fig. 2), indicating that their activity was enhanced by increasing temperature. At the species level, we also found that the abundances of several MAGs belonging to *Burkholderiales* (*Pandoraea*: bin37; *Cupriavidus*: bin47, bin48) or *Sphingomonadales* (*Sphingobium*: bin7; *Novosphingobium*: bin14) significantly increased with increased temperature (Table S4 and S5; ALDEx2, $P < 0.05$). Moreover, *Betaproteobacteria* (*Burkholderiales*), *Alphaproteobacteria* (*Sphingomonadales*) were also reported as active lignin-decomposing taxa in permafrost [18, 34, 35]. Given the fact that *Burkholderiales* and *Sphingomonadales* were abundant in diverse ecosystems [24, 36–42], the intensified global warming might exert great threat on the recalcitrant organic carbon pool by enhancing the activity of these decomposers. Unlike previous studies [43, 44], we did not find any archaeal lignin decomposers at the ASV level based on the strict filtering threshold in our study, although the relative abundance of order *Bathyarchaea* ranged from 0.46 to 0.70% in the ^{13}C -lignin-labeled DNA samples. Additionally, the lignin decomposers that were identified in this study were also different from those in thermophilic environments, where the lignin decomposers were affiliated to *Hyphomicrobiales* (*Parvularculaceae*) and *Parvularculales* (*Parvularculaceae*) etc. [24, 25].

The HMW lignin, which is composed of phenylpropanoid units, could be decomposed into vanillin (LMW lignin) via different pathways, including β -aryl ether fragments, diarylpropane fragments, biphenyl fragments, ferulic acid fragments, Pinoresinol fragments, Phenylcoumarane fragments, Syringyl lignin fragments. Many bacteria were involved in the decomposition of HMW lignin [14, 45, 46]. These bacteria could produce several types of extracellular oxidative enzymes, such as laccases, high redox potential ligninolytic peroxidases (lignin peroxidase/A, B C type dye-decolorizing peroxidase,

versatile peroxidase), β -etherase, and Ca -dehydrogenase [12, 13, 47, 48]. We found that the transcriptional abundances of β -etherase (*ligEFG*) and Ca -dehydrogenase (*ligD*), which are key genes for β -aryl ether fragments decomposing, increased by 2.14~3.16-fold as temperature increased by 3~6 °C. Additionally, the activity of key genes for decomposing ferulic acid fragments and di-arylpropane fragments also increased as temperature increasing. However, the activity of biphenyl fragments and syringyl lignin fragments decomposing pathways was inhibited by increased temperature. In the later stage of lignin decomposition, vanillic acid/vanillin was further oxidated to protocatechuic acid by gene (*ligM*), whose activity was enhanced by increased temperature. Subsequently, the ring of protocatechuic acid could be cleaved via two main distinct pathways (*4,5-PDOG pathway*, *3,4-PDOG pathway*). The transcriptional abundances of key genes in *4,5-PDOG pathway* significantly increased with increasing temperature (Fig. 5; ALDEx2, $P < 0.05$). This enhancement could increase the inputs of acetyl-coenzyme or pyruvate for the tricarboxylic acid (TCA) cycle, consequently leading to higher carbon dioxide production. These findings demonstrated that increasing temperature could enhance the decomposition of both HMW lignin and LMW intermediates (e.g., vanillin) via increasing the activity of specific decomposing pathways (Fig. 7).

Temperature significantly influenced lignin/vanillin decomposers. The abundance of vanillin decomposers increased more than lignin decomposers under elevated temperature (Fig. 2b), likely due to its simpler chemical structure and straightforward metabolic pathways that allow for direct bacterial absorption or diffusion into cells [49]. In contrast, lignin's complex, highly cross-linked polymer structure necessitates extracellular enzyme secretion and a series of enzymatic reactions [50]. Previous studies indicated that substrate complexity dictated microbial efficiency's sensitivity to temperature [51]. The metabolic pathway for vanillin decomposition was relatively straightforward, involving fewer taxa predominantly from orders like *Burkholderiales*, *Pseudomonadales*, and *Sphingomonadales* (Fig. 2b). Conversely, lignin decomposition involved a broader range of taxa, including *Anaerolineales*, *Gemmatimonadales*, and *Actinomycetales*, responding differently to temperature changes (Fig. 3). For example, Genus *Pseudomonas* showed enhanced decomposition efficiency at higher temperatures [52]. In communities dominated by fewer decomposing taxa, the temperature response of dominant species significantly influences overall behavior. However, within more diverse decomposing communities, varied responses can offset each other, diminishing the temperature effect on decomposition rates.

It should be noted that although lignin-decomposing enzymes have been identified and characterized using model substrates (i.e., vanillin, vanillic acid), the information about how oxidized lignin fragments are broken down is incomplete, which is based upon pathways elucidated in bacteria that could decompose certain lignin components [14, 50, 53]. Therefore, lots of works are still needed for more comprehensively understanding the effects of temperature on microbial-mediated lignin decomposition. Importantly, the lignin degraders we identified belong to taxa widely present in natural environment [12, 18, 25, 48, 54], suggesting that the response to warming within these taxa may have environmental universality.

Lignin represents a highly promising resource for bio-energy production [55]. Understanding the effects of temperature increases on lignin decomposition pathways and identifying effective lignin-degrading microbial communities provide theoretical support for optimizing the biological degradation and conversion processes of lignin in industrial applications. This optimization may improve the efficiency of converting biomass into biofuels such as ethanol and butanol [56]. Additionally, lignin is a major byproduct of the papermaking process [57]. By introducing efficient lignin-decomposing microorganisms or enzymatic systems, the utilization rate of lignin can be increased, thereby reducing waste discharge. The promotion of lignin decomposing by elevated temperatures offers new insights into optimizing pulping processes. Moreover, specific microbial communities exhibit enhanced decomposition capabilities of small aromatic compounds derived from lignin under higher-temperature conditions [57, 58]. This finding provides novel perspectives for the bioremediation of aromatic pollutants.

Methods

Sediment collection and preparation

Surface (0–10 cm) sediment (~1 kg) was collected by a grab sampler from the Pearl River, upstream of the Pearl River Estuary, in China (23.1037°N, 113.3008°E) on 23th May 2021. The temperature, dissolved oxygen (DO), and conductivity of the sediment were measured on site using a HQD Field portable probes Kit (HACH 58258; Loveland, Colorado, USA). In the laboratory, the pore-water was removed from the sediment by centrifuging. Then, the sediment was placed into the lightproof bottle for stable isotope probing (SIP) experiment.

The stable isotope probing experiments

Two ^{13}C -labeled substrates (^{13}C -lignin and ^{13}C -vanillin) were selected for SIP incubation experiments. ^{13}C -lignin was used to indicate the decomposition of HMW lignin in the early stages (lignin macromolecular polymer

decomposed into smaller aromatic compounds), while ^{13}C -vanillin was used to indicate later stage of lignin decomposition (ring cleavage of aromatic compounds).

^{13}C -lignin experiment: [U- ^{13}C]-Lignin (97 atom % ^{13}C ; ISOREAG[®], Netherlands, Catalog No. IR-40024, Lot No.21B043-A3), which was used as the stable isotope probe substrate, was composed of coumarin ($^{13}\text{C}_9\text{H}_{10}\text{O}_2$), coniferol ($^{13}\text{C}_{10}\text{H}_{12}\text{O}_3$), and Sinerol ($^{13}\text{C}_{11}\text{H}_{14}\text{O}_4$). We also used [U- ^{12}C]-Lignin (ISOREAG[®], Netherlands, CAS. 9005–53-2, Catalog No. ZC-47020, Lot No.21J048-A1) as the control substrate. Three treatments were set: (I) 20 mg [U- ^{13}C]-lignin was uniformly mixed with 4 g sediment; (II) 20 mg [U- ^{12}C]-lignin was mixed evenly with 4 g sediment as isotope control; (III) 4 g sediment with no extra additions was used as background control.

^{13}C -vanillin experiment: ^{13}C -vanillin-(phenyl- $^{13}\text{C}_6$) (99 atom% ^{13}C ; ISOREAG[®], Netherlands, CAS. 201,595–58-6, Catalog No. CLM-1515–0, Lot No. PR-29840) was used as the stable isotope probe substrate and ^{12}C -vanillin (ISOREAG[®], Netherlands, CAS. 121–33-5, Catalog No. ZC-53277, Lot No. 21J048-A2) was used as a control substrate. Three treatments were set: (I) 0.5 mL 0.5% ^{13}C -vanillin dissolved in 4 g sediment (0.5 mg/g w/w) as isotope treatment; (II) 0.5 mL 0.5% ^{12}C -vanillin dissolved in 4 g sediment as isotope control; (III) 0.5 mL water with 4 g sediment was used as background control.

Three temperature conditions (23 °C, 26 °C, and 29 °C) were set for each treatment and three biological replicates were set under each temperature condition. Each replicate was sealed in a 25 mL lightproof bottle and incubated for 42 days (^{13}C -lignin experiment) or 6 days (^{13}C -vanillin experiment) (Fig. 1a). We determined the experimental temperature according to the average temperature (~23 °C) observed during the current summer (April to November) at the sampling site and the projected global warming (increasing ~3 °C to 6 °C) in the next hundred years, as indicated in the IPCC reports [59].

CO₂ flux measurement

During the incubations, 10 mL of headspace gas from each bottle was daily collected using 10 mL aluminum mold vacuum gas sampling bags with valve. To balance the negative pressure relative to atmospheric pressure, one syringe was used to drain the gas from the bottle while another syringe was used to inject 10 mL helium into each bottle to equalize the pressure. Afterward, the bottles were opened and refreshed for 30 min. CO₂ flux in units of mole fraction (ppm) was measured using cavity ring-down spectroscopy (CRDS, Picarro G2201-i) at a frequency of 1 Hz [60]. The measured concentrations of CO₂ and $^{13}\text{CO}_2$ in ppm were transformed into the number of moles (n) using the ideal gas law equation $PV=nRT$, where P (pressure) was 101 kPa; V (volume)

was 25 mL multiplying the obtained CO₂ or ¹³CO₂ concentration in parts per million; R (the gas constant) was 8.314 J K⁻¹ mol⁻¹, and T (temperature) was 298 K. The Pee Dee Belemnite (PDB), a Cretaceous marine fossil of *Belemnitella americana* from the Peedee Formation in South Carolina, served as the standard for ¹³CO₂. The isotope data were reported as delta values relative to a standard, in units of “per mil” (parts per thousand). The delta notation (δ-notation) for the value of ¹³C is:

$$\delta^{13}\text{C} = \left[\frac{\frac{^{13}\text{C}}{^{12}\text{C}} (\text{Sample})}{\frac{^{13}\text{C}}{^{12}\text{C}} (\text{Reference})} - 1 \right] * 1000$$

The percentage of the CO₂-C derived from lignin/vanillin was calculated as:

$$\%C_{\text{substrate}} = \frac{\delta_{\text{C}} - \delta_{\text{T}}}{\delta_{\text{C}} - \delta_{\text{L}}} \times 100\%$$

where δ_C is the δ¹³C value of respired CO₂ from the sediment with no added lignin/vanillin, δ_T is the δ¹³C value of respired CO₂ from the sediment with ¹³C-lignin/¹³C-vanillin, and δ_L is the δ¹³C value of ¹³C-lignin/¹³C-vanillin. Because vanillin was added to the sediment in the form of water solution, the amount of sediment organic matter C primed by vanillin was calculated as total sediment respiration after vanillin addition minus the amount of C respired from vanillin, and then minus the amount of C primed by water (C respired from the sediment with no added vanillin).

Extraction of sediment DNA and RNA

After incubation of 42 or 6 days for the stable isotope probing experiment, total 54 samples (2 ¹³C-substrates × 3 treatments × 3 temperature conditions × 3 replicates) were collected for DNA and RNA extraction. The total DNA and RNA was extracted by using the QIAGEN[®] Total RNA Isolation Kit (QIAGEN, Germany). RNA was eluted from the RNA capture column by RNeasy PowerSoil Total RNA Kit (QIAGEN[®], Germany). We removed DNA contamination from the extracted RNA using the TURBO DNA-free[™] Kit (Life Technologies, Austin, TX, USA). DNA was eluted from the RNA capture columns using the RNeasy PowerSoil DNA Elution Kit (QIAGEN[®], Germany). The extracted DNA was subsequently utilized for density gradient ultra-centrifugation and qPCR experiments.

¹³C-DNA separation

According to previously established protocol [61], the extracted DNAs from ¹³C-lignin/vanillin and ¹²C-lignin/vanillin added samples (total 36 = 4 treatments × 3 temperature conditions × 3 replicates) were used for density

gradient hypervelocity centrifugation [62]. For each sample, 2.5 μg DNA was mixed with a CsCl solution with an initial buoyant density of 1.4008 g/mL (25 °C) in 4.9 mL OptiSeal polyallomer tubes (Beckman Coulter, Palo Alto, USA). The mixture was centrifuged at 408,500 g for 48 h at 20 °C in an Optima XPN-100 ultracentrifuge (Beckman Coulter) equipped with a VTi 90 vertical rotor (Beckman Coulter, USA) [63]. The DNA gradients were fractionated into 24 equal volumes (~200 μL) utilizing a fraction recovery system (Beckman Coulter, USA). The buoyant density of each fraction was determined by measuring the refractive index with a digital refractometer (Palette, ATAGO, Japan). DNA was precipitated from CsCl using glycogen (6 μL; ZOMANBIO, China) in 30% ethanol and subsequently was eluted with 30 μL TE buffer (pH 8.0) [63].

Quantitative PCR (qPCR) was utilized to quantify 16S rRNA gene copy number in each density fraction. The V3 region of the 16S rRNA genes was targeted using universal primers 338F (5'-ACTCCTACGGGAGGCAGCAG-3') and 518R (5'-ATTACCGCGGCTGCTGG-3'). qPCR was conducted in triplicate 25 μL reactions containing 10 μL Universal SYBR[®] Green Supermix (Bio-Rad, Hercules, CA, USA), 400 nM each primer and 2 μL DNA template. The thermal cycling program was carried out on a CFX96 Real-time PCR Detection System (Bio-Rad, Hercules, CA, USA), consisting of a 15-min pre-denaturation step, followed by 40 cycles with the following settings: 95 °C for 30 s, 60 °C for 30 s, and 72 °C for 30 s. Gene copy numbers were determined by a standard curve constructed with 16S rRNA gene segment of *Escherichia coli* competent cells and TA cloning vector (Promega, Madison, WI, USA). According to the buoyant density and the distribution of 16S rRNA gene copy number, the DNA in light fractions was identified as ¹²C-labeled DNA, while the DNA in heavy fractions was identified as ¹³C-labeled DNA.

Amplicon sequencing and analyses

As for the amplification of 16S rRNA gene, we used both DNA and cDNA as templates. DNA templates included the ¹³C-labeled DNA from ¹³C-lignin/vanillin added treatments (18 samples) and total DNA from all other treatments (36 samples). Additionally, cDNA templates came from the reverse transcription of the extracted RNA from all (54) samples using an M-MLV first strand cDNA Synthesis Kit (Omega BioTek, Doraville, GA, USA). During gel electrophoresis detection, no target bands were observed in all negative control samples. Following the previously described methods [64], 16S rRNA gene was amplified using the primer set: 515F-Y (5'-GTGYCAGCMGCCGCGGTAA-3') and 926R (5'-CCGYCAATTYMTTTRAGTTT-3'). The PCR products were

pooled in equal molar concentration and purified by the E.Z.N.A. gel extraction kit (Omega BioTek, Doraville, GA, USA). Amplicons were subsequently sequenced on the Illumina NovaSeq 6000 PE250 platform by MAGI-GENE (Guangzhou, China).

The 16S rRNA gene amplicons sequencing data were processed as previously described [65]. Briefly, we merged pair-end reads using USEARCH v11 and removed primers using CUTADAPT v2.4 software (parameter “–no-indels-e 0 –discard-unrimmed”) [66]. Then, low-quality reads (length < 350 bp or maximum expected error > 1.0) were further filtered out and the remained high-quality reads were clustered into amplicon sequence variants (ASVs) using unoise3 algorithm [67]. The taxonomy of ASVs were determined by Naïve Bayes Classifier [68] against SILVA 138 database in the QIIME2 platform [69]. After removing ASVs that were not classified into bacteria or archaea, we obtained ASVs table by mapping primers-removed reads to the representative sequences of ASVs. The range of sequencing depths we obtained was from 38,956 reads to 163,751 reads. The ASVs table was rarefied to the lowest reads number (38,956) of all samples to correct the effect of different sequencing depths. The reads count of each ASV was divided by its 16S rRNA gene copy number, which was obtained by utilizing the rrnDB database (<https://rrndb.umms.med.umich.edu/>). The 16S rRNA-gene-copy-number-corrected ASV count table was then converted into a relative abundance table. Finally, the absolute abundances of ASVs in each sample were computed by multiplying their relative abundances by the total 16S rRNA gene copy number of that sample, which was determined by qPCR technique. The potential lignin/vanillin decomposers were identified at ASV level from the ¹³C-labeled microbial communities with two criteria: (1) occurred in all replicates of the same treatments; (2) the relative abundance greater than 0.1% in at least one replicate sample. A maximum likelihood phylogenetic tree was constructed based on the representative sequences of these identified potential lignin/vanillin decomposers using MEGA X software [70]. The visualization of the final tree was performed using iTOL [71].

Metagenomic and metatranscriptomic analyses

Total 9 ¹³C-labeled DNA samples (1 ¹³C-vanillian added treatment × 3 temperature conditions × 3 replicates) and 18 RNA samples (2 ¹³C-lignin/vanillin added treatments × 3 temperature conditions × 3 replicates) were sequenced on the Illumina NovaSeq 6000 PE150 platform. The metagenomic sequencing data were processed as previously documented [72]. Briefly, we removed low-quality reads and adapters from raw metagenomic data using fastp v0.23.4 [73] and assembled high-quality reads into scaffolds using SPAdes v 3.15.2 [74]. Open

reading frames (ORFs) were predicted from all scaffolds (> 500 bp) using Prodigal v2.6.3 [75]. All predicted ORFs were clustered into non-redundant gene catalogue using CD-HIT-EST v4.8.1 with parameters “–c 0.95 –aS 0.9.” As for metatranscriptomic data, we removed low-quality reads and adapters using fastp v0.23.4 and removed rRNA reads using RiboDetector [76] with parameter “–e rrna.” Then, the abundances and transcriptional abundances, which was calculated as RPKM (Reads per Kilobase per million mapped reads), of each ORF across samples were determined by mapping high-quality metagenomic and metatranscriptomic reads to non-redundant gene catalogue using Bowtie2 v2.5.1 [77] and CoverM v0.6.1 (<https://github.com/wwood/CoverM>) with parameters “–min-read-percent-identity 0.95 –min-read-aligned-percent 0.80 –min-covered-fraction 0.60.” Additionally, the Metagenome-Assembled Genomes (MAGs) were recovered from metagenomic data and refined by using MetaWRAP software [78]. The qualities of MAGs were assessed using CheckM v.1.0.12 [79]. PROKKA v.1.12 [80] was utilized to annotate all medium-to-high quality MAGs (completeness > 60% and contamination < 5%).

Construction of lignin and vanillin metabolic pathway

A comprehensive collection of enzyme protein sequences associated with lignin decomposition was curated from published articles (Table S3). The non-redundant gene catalogue was then searched against these protein sequences using DIAMOND v0.9 with parameters “–id 50–query-cover 80” [81]. The RPKMs of all ORFs that were annotated to the same functional (lignin/vanillin decomposition) gene were summed to represent the abundance of this functional gene. The transcriptional abundances of these functional genes were employed to indicate the activity of the related lignin/vanillin decomposition pathways. Additionally, we identified the MAGs that were potentially involved in lignin decomposition by searching the predicted ORFs of each MAG against the previously obtained lignin-decomposition-related protein sequences using DIAMOND v0.9. These MAGs were then assigned to the specific lignin decomposition pathway based on the functional genes they contained.

To determine the taxonomy of lignin/vanillin decomposition related functional genes, we searched them against the GTDB r95 protein database using DIAMOND v0.9 with the parameters “–evaluate 0.00001-k 10.” The top 10 hits were used to determine the taxonomy of each functional gene according to the Last Common Ancestor (LCA) method. To ensure consistency between different databases, the GTDB taxonomy was converted into the NCBI taxonomy using the mapping file provided by GTDB.

Furthermore, we searched the non-redundant gene catalogue against the carbon decomposition genes database [18] to investigate the effects of temperature on the abundances and transcriptional abundances of broad carbon decomposing genes.

Isolation and identification of lignin decomposers

After serial dilution of sediment, enrichment cultures were conducted using lignin as the sole carbon source, followed by plate isolation. The detailed processes are as follows: sediments (0.1 g each) were supplemented with 4 mL BMM culture medium (sterile water), resulting in total 80 mL volume. After incubation on a shaker for 2 h, gradient dilutions were performed by transferring 1 mL sample to tube A (10^{-1}) with 9 mL modified BMM medium [35] (Table S7). Subsequently, 1 mL diluted sample from tube A was added to tube B (10^{-2}) with 9 mL BMM medium. Three replicate controls were set, and the culture solution was monitored for bacterial growth every 3 days, while the enriched solution was sampled every 15 days. After gradient dilutions, lignin was used as the sole carbon source, and the culture was carried out in a modified BMM medium. Lignin-decomposing strains were isolated by BMM medium plate purification after two weeks (Fig. S7).

The DNA of two isolated bacterial strains based on the previous methods [82] were then sequenced on the Illumina Nova PE150 platform. The low-quality reads were filtered out by fastp v0.23.2 [73] and the remained high-quality reads were assembled into draft genomes by SPAdes v3.15.2 [74]. Genomes' qualities were evaluated by CheckM v1.2.2 [79] and genomes were annotated by PROKKA v1.12 [80] was employed. To identify whether these three isolated strains contained any known lignin-decomposition-related genes, we searched the predicted ORFs from each genome to previously acquired lignin-decomposition-related protein sequences using DIAMOND v0.9 [81].

Statistical analyses

The differences in bacterial copy number between the different treatments were assessed using the Kruskal–Wallis test. To ensure accurate normalization across different taxonomic groups, information on 16S rRNA gene copy numbers for each ASV was adjusted from the rrnDB database (<https://rrndb.umms.med.umich.edu/>) [83]. The ALDEx2 R package was used to determine the differences in the abundance of ASVs and MAGs among samples subjected to different temperature treatments. Multivariate statistical tests (PERMANOVA) and Non-Metric Multidimensional Scaling (NMDS) based on “Bray–Curtis dissimilarity” were used to illustrate the similarity distributions of lignin/vanillin decomposers

community. The one-way ANOVA test was used to determine the differences in CO₂ productions among samples with different temperature conditions. Mean values were reported as mean ± SD, unless otherwise specified, and significance was defined as $P < 0.05$. All the above analyses were conducted using R software (version 4.2.2).

Conclusion

In this study, we demonstrated that temperature had notable effects on microbial-mediated lignin/vanillin decomposition utilizing SIP experiments and multi-omics techniques. As the temperature increased, microbial respiration, lignin/vanillin decomposition, and priming effect were all enhanced. Meanwhile, the decomposition of lignin/vanillin may be more sensitive to temperature changes than other organic carbons. We also identified that *Burkholderiales*, *Sphingomonadales*, and *Pseudomonadales* were the main potential lignin/vanillin decomposers, and their abundances changed significantly as the temperature increased. Additionally, we found that the activity of several decomposing pathways, including *β-aryl ether* and *4,5-PDOG pathway*, significantly increased with increasing temperature. To our knowledge, this study provided the first comprehensive report about the effects of temperature on microbial-mediated lignin/vanillin decomposition in river sediment. Our findings indicate that the ongoing intensification of global warming may accelerate the decomposition of recalcitrant organic carbon via increasing microbial activity in river sediment, thereby impacting global carbon cycling.

Supplementary Information

The online version contains supplementary material available at <https://doi.org/10.1186/s40168-025-02076-z>.

Supplementary Material 1: Fig. S1 Detection of 13C-labelled DNA in density gradient fractions using qPCR targeting 16S rRNA genes. Fig. S2 Detection of 13C-labelled DNA in density gradient fractions using qPCR targeting 16S rRNA genes. Fig. S3 The changes of bacterial community compositions with temperature increasing. Fig. S4. The changes in relative abundances of potential lignin/vanillin microbial decomposers under different temperature conditions (a: lignin; b: vanillin). Fig. S5 The effects of temperature on lignin and vanillin decomposition pathways. (a) Lignin decomposition pathways under different temperatures. (b) Vanillin decomposition pathways under different temperatures. Fig. S6 Diversity changes of microbial community to increasing temperature. Fig. S7 Isolation cultivation of lignin-decomposing bacteria strains

Supplementary Material 2: Table S1. The accumulated 13CO₂ and total CO₂ during the 42 days lignin incubation experiment. Table S2. The accumulated 13CO₂ and total CO₂ during the 6 days vanillin incubation experiment. Table S3. Information of lignin-decomposition related gene. Table S4. Summary information of the high-quality MAGs in 13C-labeled DNA. Table S5. The presence (1) and absence (0) of lignin-decomposition related gene in the high-quality MAGs from 13C-labeled DNA. Table S6. Lignin-decomposition related genes in the genomes of isolated strains. Table S7. List of specific components in the BMM-defined medium

Acknowledgements

We thank Xuanyu Tao and Ruoyun Wang for their assistance during the study.

Authors' contributions

J.L., W.L., and P.W. conceived this study. J.L. and J.W. collected the samples. J.L., L.D., X.L., Q.D. and Z.P. carried out the incubation, and the related gas experiment. W.S. and M. Z. provided technology for isotope cultivation and fractionation experiments. Y.C. provided the platform and technology for isotope gas detection. P.W. and J.L. conducted bioinformatic analysis. J.L. wrote the first draft manuscript. J.L., P.W. and X.M. edited and revised the manuscript with contributions and inputs from all authors.

Funding

This work was supported by the National Natural Science Foundation of China (Nos. 32200090, 32400095), Guangdong S&T Program (2022B0202110001), and Guangdong Basic and Applied Basic Research Foundation, China (Nos. 2023A1515012270, 2025A1515010895).

Data availability

No datasets were generated or analysed during the current study.

Declarations

Ethics approval and consent to participate

Not applicable.

Consent for publication

Not applicable.

Competing interests

The authors declare no competing interests.

Author details

¹State Key Laboratory of Biocontrol, Guangdong Provincial Key Laboratory of Plant Stress Biology, School of Environmental Science and Engineering, School of Life Sciences, School of Ecology, Sun Yat-Sen University, Guangzhou, Guangdong 510275, China. ²Southern Marine Science and Engineering Guangdong Laboratory (Guangzhou), Guangzhou 511458, China. ³Institute of Eco-Environmental and Soil Sciences, Guangdong Academy of Sciences, Guangzhou 510650, China. ⁴Key Laboratory of Water Quality and Conservation in the Pearl River Delta, Ministry of Education, School of Environmental Science and Engineering, Guangzhou University, Guangzhou 510006, China. ⁵Department of Biological Sciences, Kent State University, Kent, OH 44242, USA. ⁶School of Pharmacy, Shenzhen University Medical School, Shenzhen University, Shenzhen 518055, China.

Received: 5 December 2023 Accepted: 4 March 2025

Published online: 01 April 2025

References

- Battin TJ, Lauerwald R, Bernhardt ES, Bertuzzo E, Gener LG, Hall RO Jr, Hotchkiss ER, Maavara T, Pavelsky TM, Ran L, et al. River ecosystem metabolism and carbon biogeochemistry in a changing world. *Nature*. 2023;613(7944):449–59.
- Ni HG, Lu FH, Luo XL, Tian HY, Zeng EY. Riverine inputs of total organic carbon and suspended particulate matter from the Pearl River Delta to the coastal ocean off South China. *Mar Pollut Bull*. 2008;56(6):1150–7.
- Mendonca R, Muller RA, Clow D, Verpoorter C, Raymond P, Tranvik LJ, Sobek S. Organic carbon burial in global lakes and reservoirs. *Nat Commun*. 2017;8(1):1694.
- Bao H, Wu Y, Zhan X, Wang X, Spencer RGM, Hernes PJ, Feng X, Lee LC, Huang JC, Zhang J, et al. Global riverine export of dissolved lignin constrained by hydrology, geomorphology, and land-cover. *Glob Biogeochem Cycles*. 2023;37(4):e2022GB007607.
- Freixa A, Acuña V, Casellas M, Pecheva S, Romani AM. Warmer night-time temperature promotes microbial heterotrophic activity and modifies stream sediment community. *Glob Change Biol*. 2017;23(9):3825–37.
- Liu S, Xie Z, Liu B, Wang Y, Gao J, Zeng Y, Xie J, Xie Z, Jia B, Qin P, et al. Global river water warming due to climate change and anthropogenic heat emission. *Glob Planet Change*. 2020;193:103289.
- Hemingway JD, Schefub E, Spencer RGM, Dinga BJ, Eglinton TI, McIntyre C, Galy VV. Hydrologic controls on seasonal and inter-annual variability of Congo River particulate organic matter source and reservoir age. *Chem Geol*. 2017;466:454–65.
- Davidson EA, Janssens IA. Temperature sensitivity of soil carbon decomposition and feedbacks to climate change. *Nature*. 2006;440(7081):165–73.
- Asina F, Brzozova I, Voeller K, Kozliak E, Kubátová A, Yao B, Ji Y. Bio-degradation of lignin by fungi, bacteria and laccases. *Biores Technol*. 2016;220:414–24.
- Ward ND, Keil RG, Medeiros PM, Brito DC, Cunha AC, Dittmar T, Yager PL, Krusche AV, Richey JE. Degradation of terrestrially derived macromolecules in the Amazon River. *Nat Geosci*. 2013;6(7):530–3.
- Woo HL, Hazen TC. Enrichment of bacteria from eastern mediterranean sea involved in lignin degradation via the phenylacetyl-CoA pathway. *Front Microbiol*. 2018;9:922.
- Xu R, Zhang K, Liu P, Han H, Zhao S, Kakade A, Khan A, Du D, Li X. Lignin depolymerization and utilization by bacteria. *Biores Technol*. 2018;269:557–66.
- Subbotina E, Rukkijakan T, Marquez-Medina MD, Yu X, Johnsson M, Samec JSM. Oxidative cleavage of C–C bonds in lignin. *Nat Chem*. 2021;13(11):1118–25.
- Bugg TD, Ahmad M, Hardiman EM, Rahmanpour R. Pathways for degradation of lignin in bacteria and fungi. *Nat Prod Rep*. 2011;28(12):1883–96.
- Watts JEM, McDonald RC, Schreier HJ. Wood degradation by *Panaque nigrolineatus*, a neotropical catfish: diversity and activity of gastrointestinal tract lignocellulolytic and nitrogen fixing communities. *Wood Degrad Ligninolytic Fungi*. 2021;99:209–38. <https://doi.org/10.1016/bs.abr.2021.05.005>.
- Pold G, Melillo JM, DeAngelis KM. Two decades of warming increases diversity of a potentially lignolytic bacterial community. *Front Microbiol*. 2015;6:480.
- Dutschei T, Beidler I, Bartosik D, Seesselberg JM, Teune M, Baumgen M, Ferreira SQ, Heldmann J, Nagel F, Krull J, et al. Marine Bacteroidetes enzymatically digest xylans from terrestrial plants. *Environ Microbiol*. 2023;25(9):1713–27.
- Tao X, Feng J, Yang Y, Wang G, Tian R, Fan F, Ning D, Bates CT, Hale L, Yuan MM, et al. Winter warming in Alaska accelerates lignin decomposition contributed by Proteobacteria. *Microbiome*. 2020;8(1):84.
- Wilhelm RC, Singh R, Eltis LD, Mohn WW. Bacterial contributions to delignification and lignocellulose degradation in forest soils with metagenomic and quantitative stable isotope probing. *ISME J*. 2019;13(2):413–29.
- Salvachua D, Werner AZ, Pardo I, Michalska M, Black BA, Donohoe BS, Haugen SJ, Katahira R, Notonier S, Ramirez KJ, et al. Outer membrane vesicles catabolize lignin-derived aromatic compounds in *Pseudomonas putida* KT2440. *Proc Natl Acad Sci USA*. 2020;117(17):9302–10.
- Li JL, Duan L, Wu Y, Ahmad M, Yin LZ, Luo XQ, Wang X, Fang BZ, Li SH, Huang LN, et al. Unraveling microbe-mediated degradation of lignin and lignin-derived aromatic fragments in the Pearl River Estuary sediments. *Chemosphere*. 2022;296:133995.
- Wu Y, Bao H, Yu H, Zhang J. Kattner aG: Temporal variability of particulate organic carbon in the lower Changjiang (Yangtze River) in the postThree Gorges Dam period: Links to anthropogenic and climate impacts. *J Geophys Res: Biogeosciences*. 2015;120:2194–211.
- Li J, Wang P, Salam N, Li X, Ahmad M, Tian Y, Duan L, Huang L, Xiao M, Mou X, et al. Unraveling bacteria-mediated degradation of lignin-derived aromatic compounds in a freshwater environment. *Sci Total Environ*. 2020;749:141236.
- Levy-Booth DJ, Hashimi A, Roccor R, Liu LY, Rennecker S, Eltis LD, Mohn WW. Genomics and metatranscriptomics of biogeochemical cycling and degradation of lignin-derived aromatic compounds in thermal swamp sediment. *ISME J*. 2021;15(3):879–93.
- Levy-Booth DJ, Navas LE, Fetherolf MM, Liu LY, Dalhuisen T, Rennecker S, Eltis LD, Mohn WW. Discovery of lignin-transforming bacteria and enzymes in thermophilic environments using stable isotope probing. *ISME J*. 2022;16(8):1944–56.
- Tareq SM, Tanaka N, Ohta K. Biomarker signature in tropical wetland: lignin phenol vegetation index (LPVI) and its implications

- for reconstructing the paleoenvironment. *Sci Total Environ.* 2004;324(1–3):91–103.
27. Xue K, Yuan MM, Shi ZJ, Qin YJ, Deng Y, Cheng L, Wu LY, He ZL, Van Nostrand JD, Bracho R, et al. Tundra soil carbon is vulnerable to rapid microbial decomposition under climate warming. *Nat Climate Change.* 2016;6(6):595–+.
 28. Sorensena PO, Finzia AC, Giassona M-A, Reinmanna AB, Sanders-DeMotta R, Templera PH. Winter soil freeze-thaw cycles lead to reductions in soil microbial biomass and activity not compensated for by soil warming. *Soil Biol Biochem.* 2018;116:39–47.
 29. Yuan MM, Guo X, Wu LW, Zhang Y, Xiao NJ, Ning DL, Shi Z, Zhou XS, Wu LY, Yang YF, et al. Climate warming enhances microbial network complexity and stability. *Nat Clim Chang.* 2021;11(4):343–U100.
 30. Guo X, Feng JJ, Shi Z, Zhou XS, Yuan MT, Tao XY, Hale L, Yuan T, Wang JJ, Qin YJ, et al. Climate warming leads to divergent succession of grassland microbial communities. *Nat Climate Change.* 2018;8(9):813–+.
 31. Zheng ZZ, Zheng LW, Xu MN, Tan E, Hutchins DA, Deng W, Zhang Y, Shi D, Dai M, Kao SJ. Substrate regulation leads to differential responses of microbial ammonia-oxidizing communities to ocean warming. *Nat Commun.* 2020;11(1):3511.
 32. Chen J, Luo Y, Garcia-Palacios P, Cao J, Dacal M, Zhou X, Li J, Xia J, Niu S, Yang H, et al. Differential responses of carbon-degrading enzyme activities to warming: Implications for soil respiration. *Glob Change Biol.* 2018;24(10):4816–26.
 33. Li F, Peng Y, Chen L, Yang G, Abbott BW, Zhang D, Fang K, Wang G, Wang J, Yu J, et al. Warming alters surface soil organic matter composition despite unchanged carbon stocks in a Tibetan permafrost ecosystem. *Funct Ecol.* 2020;34(4):911–22.
 34. Bastida F, Eldridge DJ, Garcia C, Kenny Png G, Bardgett RD, Delgado-Baquerizo M. Soil microbial diversity-biomass relationships are driven by soil carbon content across global biomes. *ISME J.* 2021;15(7):2081–91.
 35. Woo HL, Hazen TC, Simmons BA, DeAngelis KM. Enzyme activities of aerobic lignocellulolytic bacteria isolated from wet tropical forest soils. *Syst Appl Microbiol.* 2014;37(1):60–7.
 36. Yang X, Zhang L, Chen Y, He Q, Liu T, Zhang G, Yuan L, Peng H, Wang H, Ju F. Micro(nano)plastic size and concentration co-differentiate nitrogen transformation, microbiota dynamics, and assembly patterns in constructed wetlands. *Water Res.* 2022;220:118636.
 37. Wu D, Zhao J, Su Y, Yang M, Dolfing J, Graham DW, Yang K, Xie B. Explaining the resistomes in a megacity's water supply catchment: roles of microbial assembly-dominant taxa, niched environments and pathogenic bacteria. *Water Res.* 2023;228(Pt A):119359.
 38. Sun H, Xia J, Wu B, Ren H, Zhang X, Ye L. Aerobic starvation treatment of activated sludge enhances the degradation efficiency of refractory organic compounds. *Water Res.* 2022;224:119069.
 39. Sieradzki ET, Nuccio EE, Pett-Ridge J, Firestone MK. Expression of macromolecular organic nitrogen degrading enzymes identifies potential mediators of soil organic N availability to an annual grass. *ISME J.* 2023;17(7):967–75.
 40. Gu Y, Banerjee S, Dini-Andreote F, Xu Y, Shen Q, Jousset A, Wei Z. Small changes in rhizosphere microbiome composition predict disease outcomes earlier than pathogen density variations. *ISME J.* 2022;16(10):2448–56.
 41. Brisbin MM, Mitarai S, Saito MA, Alexander H. Microbiomes of bloom-forming *Phaeocystis* algae are stable and consistently recruited, with both symbiotic and opportunistic modes. *ISME J.* 2022;16(9):2255–64.
 42. Ling F, Hwang C, LeChevallier MW, Andersen GL, Liu W-T. Core-satellite populations and seasonality of water meter biofilms in a metropolitan drinking water distribution system. *ISME J.* 2016;10(3):582–95.
 43. Yu T, Wu W, Liang W, Lever MA, Hinrichs KU, Wang F. Growth of sedimentary Bathyarchaeota on lignin as an energy source. *Proc Natl Acad Sci USA.* 2018;115(23):6022–7.
 44. Hou J, Wang Y, Zhu P, Yang N, Liang L, Yu T, Niu M, Konhauser K, Woodcroft BJ, Fengping W. Taxonomic and carbon metabolic diversification of Bathyarchaeia during its coevolution history with early Earth surface environment. *Sci Adv.* 2023;9(27):eadf5069.
 45. Ahmad M, Taylor CR, Pink D, Burton K, Eastwood D, Bending GD, Bugg TD. Development of novel assays for lignin degradation: comparative analysis of bacterial and fungal lignin degraders. *Mol BioSyst.* 2010;6(5):815–21.
 46. Ayuso-Fernandez I, Ruiz-Duenas FJ, Martinez AT. Evolutionary convergence in lignin-degrading enzymes. *Proc Natl Acad Sci USA.* 2018;115(25):6428–33.
 47. Perez-Anton M, Schneider I, Kroll P, Hofhuis H, Metzger S, Pauly M, Hay A. Explosive seed dispersal depends on SPL7 to ensure sufficient copper for localized lignin deposition via laccases. *Proc Natl Acad Sci USA.* 2022;119(24):e2202287119.
 48. Wang X, Lin L, Zhou J. Links among extracellular enzymes, lignin degradation and cell growth establish the models to identify marine lignin-utilizing bacteria. *Environ Microbiol.* 2021;23(1):160–73.
 49. Fuchs G, Boll M, Heider J. Microbial degradation of aromatic compounds—from one strategy to four. *Nat Rev Microbiol.* 2011;9(11):803–16.
 50. Atiweh G, Parrish CC, Banoub J, Le TT. Lignin degradation by microorganisms: a review. *Biotechnol Prog.* 2022;38(2):e3226.
 51. Frey SD, Lee J, Melillo JM, Six J. The temperature response of soil microbial efficiency and its feedback to climate. *Nat Clim Change.* 2013;3(4):395–8.
 52. El-Naas MH, Al-Muhtaseb SA, Makhlof S. Biodegradation of phenol by *Pseudomonas putida* immobilized in polyvinyl alcohol (PVA) gel. *J Hazard Mater.* 2009;164(2):720–5.
 53. Reshmy R, Athiyaman Balakumaran P, Divakar K, Philip E, Madhavan A, Pugazhendhi A, Sirohi R, Binod P, Kumar Awasthi M, Sindhu R. Microbial valorization of lignin: prospects and challenges. *Biores Technol.* 2022;344(Pt A):126240.
 54. Pascual-García A, Bell T. Community-level signatures of ecological succession in natural bacterial communities. *Nat Commun.* 2020;11(1):2386.
 55. Gillet S, Aguedo M, Petitjean L, Morais ARC, da Costa Lopes AM, Lukasik RM, Anastas PT. Lignin transformations for high value applications: towards targeted modifications using green chemistry. *Green Chem.* 2017;19(18):4200–33.
 56. Bajwa DS, Pourhashem G, Ullah AH, Bajwa SG. A concise review of current lignin production, applications, products and their environmental impact. *Ind Crops Prod.* 2019;139:111526.
 57. Haq I, Mazumder P, Kalamdhad AS. Recent advances in removal of lignin from paper industry wastewater and its industrial applications—a review. *Biores Technol.* 2020;312:123636.
 58. Erickson E, Bleem A, Kuatsjah E, Werner AZ, DuBois JL, McGeehan JE, Eltis LD, Beckham GT. Critical enzyme reactions in aromatic catabolism for microbial lignin conversion. *Nat Catal.* 2022;5(2):86–98.
 59. Tollefson J. Earth is warmer than it's been in 125,000 years, says landmark climate report. *Nature.* 2021;596(12):171–2.
 60. Li X, Yao HY, Yu YX, Cao YJ, Tang CY. Greenhouse gases in an urban river: Trend, isotopic evidence for underlying processes, and the impact of in-river structures. *J Hydrol.* 2020;591:125290.
 61. Sun X, Kong T, Li F, Haggblom MM, Kolton M, Lan L, Lau Vetter MCY, Dong Y, Gao P, Kostka JE, et al. *Desulfurivibrio* spp. mediate sulfur-oxidation coupled to Sb(V) reduction, a novel biogeochemical process. *The ISME J.* 2022;16(6):1547–56.
 62. Neufeld JD, Vohra J, Dumont MG, Lueders T, Manefeld M, Friedrich MW, Murrell JC. DNA stable-isotope probing. *Nat Protoc.* 2007;2(4):860–6.
 63. Zhang M, Li Z, Haggblom MM, Young L, He Z, Li F, Xu R, Sun X, Sun W. Characterization of nitrate-dependent As(III)-oxidizing communities in arsenic-contaminated soil and investigation of their metabolic potentials by the combination of DNA-stable isotope probing and metagenomics. *Environ Sci Technol.* 2020;54(12):7366–77.
 64. Duan L, Li JL, Yin LZ, Luo XQ, Ahmad M, Fang BZ, Li SH, Deng QQ, Wang P, Li WJ. Habitat-dependent prokaryotic microbial community, potential keystone species, and network complexity in a subtropical estuary. *Environ Res.* 2022;212(Pt D):113376.
 65. Wang PD, Li JL, Luo XQ, Ahmad M, Duan L, Yin LZ, Fang BZ, Li SH, Yang YC, Jiang L, et al. Biogeographical distributions of nitrogen-cycling functional genes in a subtropical estuary. *Funct Ecol.* 2022;36(1):187–201.
 66. Martin M. Cutadapt removes adapter sequences from high-throughput sequencing reads. *EMBnet J.* 2011;17(1):10–2.
 67. Edgar RC. UNOISE2: improved error-correction for Illumina 16S and ITS amplicon sequencing. *bioRxiv.* 2016.
 68. Bokulich NA, Kaehler BD, Rideout JR, Dillon M, Bolyen E, Knight R, Huttley GA, Caporaso JG. Optimizing taxonomic classification of marker-gene amplicon sequences with QIIME 2's q2-feature-classifier plugin. *Microbiome.* 2018;6:90.
 69. Bolyen E, Rideout JR, Dillon MR, Bokulich NA, Abnet CC, Al-Ghalith GA, Alexander H, Alm EJ, Arumugam M, Asnicar F, et al. Reproducible,

- interactive, scalable and extensible microbiome data science using QIIME 2. *Nat Biotechnol.* 2019;37(8):852–7.
70. Kumar S, Stecher G, Li M, Knyaz C, Tamura K. MEGA X: Molecular Evolutionary Genetics Analysis across Computing Platforms. *Mol Biol Evol.* 2018;35(6):1547–9.
 71. Letunic I, Bork P. Interactive Tree Of Life v2: online annotation and display of phylogenetic trees made easy. *Nucleic Acids Res.* 2011;39(Web Server issue):W475–478.
 72. Luo XQ, Wang P, Li JL, Ahmad M, Duan L, Yin LZ, Deng QQ, Fang BZ, Li SH, Li WJ. Viral community-wide auxiliary metabolic genes differ by lifestyles, habitats, and hosts. *Microbiome.* 2022;10(1):190.
 73. Chen S, Zhou Y, Chen Y, Gu J. fastp: an ultra-fast all-in-one FASTQ preprocessor. *Bioinformatics.* 2018;34(17):i884–90.
 74. Nurk S, Meleshko D, Korobeynikov A, Pevzner PA. metaSPAdes: a new versatile metagenomic assembler. *Genome Res.* 2017;27(5):824–34.
 75. Hyatt D, Chen G-L, LoCascio PF, Land ML, Larimer FW, Hauser LJ. Prodigal: prokaryotic gene recognition and translation initiation site identification. *BMC Bioinformatics.* 2010;11:119.
 76. Deng ZL, Münch PC, Mreches R, McHardy AC. Rapid and accurate identification of ribosomal RNA sequences via deep learning. *Nucleic Acids Res.* 2022;50(10):e60.
 77. Langmead B, Salzberg SL. Fast gapped-read alignment with Bowtie 2. *Nat Methods.* 2012;9(4):357–9.
 78. Uritskiy GV, DiRuggiero J, Taylor J. MetaWRAP—a flexible pipeline for genome-resolved metagenomic data analysis. *Microbiome.* 2018;6(1):158.
 79. Parks DH, Imelfort M, Skennerton CT, Hugenholtz P, Tyson GW. CheckM: assessing the quality of microbial genomes recovered from isolates, single cells, and metagenomes. *Genome Res.* 2015;25(7):1043–55.
 80. Seemann T. Prokka: rapid prokaryotic genome annotation. *Bioinformatics.* 2014;30(14):2068–9.
 81. Buchfink B, Xie C, Huson DH. Fast and sensitive protein alignment using diamond. *Nat Methods.* 2015;12(1):1–2.
 82. Duan L, Li JL, Li X, Dong L, Fang BZ, Xiao M, Mou X, Li WJ. *Roseibium aestuarii* sp. nov., isolated from Pearl River Estuary. *Int J Syst Evol Microbiol.* 2020;70(4):2896–900.
 83. Stoddard SF, Smith BJ, Hein R, Roller BRK, Schmidt TM. rrnDB: improved tools for interpreting rRNA gene abundance in bacteria and archaea and a new foundation for future development. *Nucleic Acids Res.* 2015;43(D1):D593–8.

Publisher's Note

Springer Nature remains neutral with regard to jurisdictional claims in published maps and institutional affiliations.